

Ethyl xanthate collector interaction with precipitated iron and copper hydroxides – Experiments and DFT simulations



A. Sarvaramini^a, F. Larachi^{a,*}, B. Hart^b

^a Department of Chemical Engineering, Université Laval, 1065 Avenue de la médecine, Québec, Québec G1V 0A6, Canada

^b Department of Earth Sciences, Surface Science Western, The University of Western Ontario, 999 Collip Circle, P.O. Box 12, London, Ontario N6G 0J3, Canada

ARTICLE INFO

Article history:

Received 24 February 2016

Received in revised form 12 April 2016

Accepted 13 April 2016

Available online 28 April 2016

Keywords:

DFT calculations

Adsorption of ethyl xanthate collector

Flotation

Iron and copper hydroxides

ABSTRACT

The interaction of ethyl xanthate collector with precipitated iron and copper hydroxides at alkaline pH was studied both experimentally and through DFT simulations. Experiments revealed that the collector had lesser affinity for interaction with iron hydroxide precipitates compared with copper hydroxide. In an attempt to comprehend the factors in favor of the higher interactions between ethyl xanthate and copper hydroxides, quantum mechanical simulations using density functional theory (DFT) have been carried out. The DFT simulation results confirmed that the interaction of ethyl xanthate with solvated copper hydroxides was more energetically favorable than with iron hydroxides. The simulations also showed that negatively-charged iron hydroxide complexes, should they arise at alkaline pH in the electrical double layer surrounding iron hydroxide precipitates, bring about no affinity *vis-à-vis* ethyl xanthate collector and quite contrarily, their formation and adsorption on the precipitate surface could inhibit the collector adsorption.

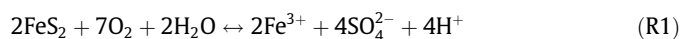
© 2016 Elsevier B.V. All rights reserved.

1. Introduction

Froth flotation is a common and versatile process used to separate the variety of minerals present in ore deposits. While the overall process mainly separates value phases from those of no or lesser value (gangue), the design of the process is more commonly optimized to selectively separate minerals of equal value to different process streams in order to minimize loss and maximize recovery of a particular commodity [1,2]. In the flotation process the surface chemistry of the various mineral phases is the essential determinant for selective separation [3–5]. With the increasingly greater occurrences of complex mineralogical ores, the interaction of the various components within the ore results in significant challenges for process control [3,6,7]. To fully optimize the control parameters for enhanced selectivity and mineral recovery, a detailed understanding of the process chemistry cannot be skipped [3–5]. During flotation, mineral surface hydrophobicity is commonly induced by the attachment of collector molecules to promote flotation [8]. Collector attachment can occur alone or, more commonly, with the assistance of an activating species [9–12]. It is well known that the reduced floatability of valuable minerals/phases can be induced by dissolution and transfer *via* solution of depressant ions to the mineral phases intended to float [9,13].

Complex interactions in the flotation pulp between the aqueous species and the mineral surfaces ultimately dictate the level whereby flotation separation will succeed or fail.

The formation of complex iron oxide/hydroxide species on chalcopyrite and pyrite surfaces is reported to considerably reduce their floatability [14–16]. There are two common sources of iron and the various iron complexes in the flotation pulp. The first source of iron in the pulp is the anodic oxidation of the steel grinding media. The process is commonly facilitated by galvanic interactions between the grinding media and sulfide minerals promoting electron transfer, stimulating corrosion of the grinding media and the release of ferric iron [17]. The second most common source is pyrite oxidation [18]. Pyrite is the most widespread sulfide mineral, when it does not host precious metals, is considered mostly as a gangue phase [7,19]. Pyrite oxidation with dissolved oxygen releases ferric iron to the pulp according to reaction (R1) [7]:



The dissolved ferric iron undergoes hydroxide complex formation to species such as $\text{Fe}(\text{OH})^{2+}$, $\text{Fe}(\text{OH})_2^+$ and $\text{Fe}(\text{OH})_3$ the stability of which primarily depends on the pulp pH and iron concentration [15]. Adsorption and/or precipitation of such complex species on the target mineral(s) could influence surface collector adsorption [7], render it hydrophilic and thus less prone to efficient flotation and recovery [8].

* Corresponding author.

E-mail address: faical.larachi@gch.ulaval.ca (F. Larachi).

The goal of the present study is to investigate the interaction of the collector ethyl xanthate with iron and copper hydroxides in alkaline solutions both through experiments and density functional theory (DFT) simulations. The study's motivation is driven by the fact that the interaction of ethyl xanthate with metal hydroxides is not well understood and therefore this study constitutes an opportunity for generating new knowledge on this crucial issue. In this regard, the research work is organized as follows. First, fixed-bed adsorption tests were carried out at pH 10 to monitor the kinetics and ultimate concentration of ethyl xanthate adsorbed on the surface of sphalerite powder. Three types of sphalerite surface modification have been investigated: pristine (clean), modified with iron hydroxide precipitates and modified with copper hydroxide precipitates. Second, the interactions between collector and metal hydroxides were then investigated theoretically by means of quantum mechanical simulations using density functional theory (DFT). The effect of water molecules as the solvent and of hydroxide anions abundant under alkaline conditions on the affinity of metal hydroxide towards collector adsorption has been also investigated.

2. Experimental and computational methodology

2.1. Materials

A sample of sphalerite, provided by Ward's National Science, was sieved to remove particles coarser than 150 μm and finer than 90 μm . The elemental composition of the sample was obtained using atomic absorption spectrometry (AAS) revealing the presence of Zn, S, Fe and Cu with the respective fractions of 58 wt%, 31 wt%, 0.28 wt% and 0.07 mg/kg. X-ray diffraction analysis of the sphalerite ore also revealed the presence of sphalerite, pyrite and silica with the respective proportions of 90 wt%, 4.7 wt% and 5.3 wt% as estimated *via* elemental analysis [20]. Prior to experiments, the oxide films on the sphalerite surface were removed by an acid wash using HCl solutions at pH 2.

All collector adsorption and flotation experiments were performed with distilled water. The reagents used in this study, copper sulfate, iron(III) chloride hexahydrate, potassium ethyl xanthate (Sigma Aldrich, 96%), sodium hydroxide (97%, VWR international) and hydrochloric acid (Laboratoire Mat) were all certified analytical grade.

2.2. Test setup

The adsorption characteristics of ethyl xanthate on the surface of different sulfide minerals such as pyrite, chalcopyrite and sphalerite as well as copper activated minerals have been studied experimentally [10,21–23]. However, the adsorption kinetics of this collector on surfaces modified by precipitated metal hydroxides has not, to the best of these authors' knowledge, been well documented in the literature. Consequently, collector adsorption characteristics on sphalerite surfaces modified by iron and copper hydroxides at alkaline (pH 10) were investigated. A schematic of the experimental setup is shown in Fig. 1.

In order to modify the sphalerite surface with selected precipitates a 150 mL solution at 1 mM of metal (Cu or Fe) at pH 10 was circulated in a closed loop for *ca.* 30 min through a fixed-bed reactor containing 4 g of sieved sphalerite grains to allow metal hydroxide precipitation and/or deposition on sphalerite. After this step, 70 mL of 32 ppm ethyl xanthate solution was passed through the sphalerite bed in a closed loop with the collector concentration monitored using a UV/Vis spectrophotometer. The collector uptake from the solution was used to demonstrate ethyl xanthate adsorption on the pristine and metal hydroxide modified sphalerite surface.

2.3. Computational assumptions

Spin unrestricted DFT calculations were carried out for the total energy calculations and the corresponding structure optimization to find the most stable geometries. Except for the electron density difference calculations, which were performed with CASTEP, all results are calculated using DMol3 package implemented in Materials Studio 7.0. DMol3 implements numerical functions on an atom-centered grid as its atomic basis and atomic basis functions are attained by solving the DFT equations for every individual atom leading to rather accurate calculations. The Perdew–Burke–Ernzerhof generalized-gradient approximation (PBE) was used to estimate the exchange–correlation energy. The core electrons were treated using DFT semi-core pseudopotentials and the double numerical plus polarization (DNP) basis set was used to develop the electronic eigenstates with an orbital cut-off radius of 4.4 Å. The self-consistent field (SCF) convergence was fixed to 10^{-6} and the convergence criteria set for the energy, maximum force and maximum displacement were 10^{-5} Ha, $2 \cdot 10^{-3}$ Ha/Å and $5 \cdot 10^{-3}$ Å, respectively. Different configurations for the interaction of ethyl xanthate and hydroxyl anions (OH^-) with the metal (copper and iron) hydroxides were studied in terms of species (molecules, ions) relaxation at different positions with respect to the metal hydroxide and the most stable configurations was hence obtained. The presence of explicit water molecules in the simulations was also considered as the solvent molecules could interact with the metal hydroxides and collectors leading to the formation of some hydrogen bonds and hydrated complexes. The interactions of explicit water solvent molecules with the metal cations, hydroxides and ethyl xanthate anion were first studied through the relaxation of only one water molecule in the different simulated cases. The number of water molecules applied in each case study was then increased one by one to investigate the effect of presence of more water molecules in the interactions between the solvents and different solute species. Using this method, the maximum number of water molecules which could directly interact with different solute species through hydrogen bonding or formation of covalent bonds between water and solute can be obtained. Further addition of more water molecules to these incremental hydrated complexes ended up into structures wherein the latter water molecules associated with the former water molecules without direct interaction with the solutes. It should be mentioned that the results presented here correspond to simulations in the presence of maximum water molecules which showed direct interaction with the solute. Depending on the cases, this number varied between four and six water molecules. The interaction energy of collector and OH^- group with the metal hydroxide was calculated through subtraction of the total energy of the system after interaction ($E_{\text{coll/OH}^- + \text{M(OH)}}$) from that of the system before interaction ($E_{\text{coll/OH}^-} + E_{\text{M(OH)}}$). In the presence of water solvent, the adsorption energy was calculated as the energy difference between the most stable interaction configuration and the configuration in which the solvated reagents have not interacted with each other. Negative adsorption energy is indicative of exothermic adsorption and strong interaction of the collector with the metal hydroxides [24–26]. Finally, the energy barriers were calculated by transition state search using the method of complete linear synchronous transit (LST)/quadratic synchronous transit (QST) implemented in DMol3.

3. Results and discussions

3.1. Kinetics of ethyl xanthate adsorption on bare and metal-hydroxide-modified sphalerite

Fig. 2 shows the kinetics of ethyl xanthate adsorption on the surface of bare and metal hydroxide modified sphalerite in alkaline

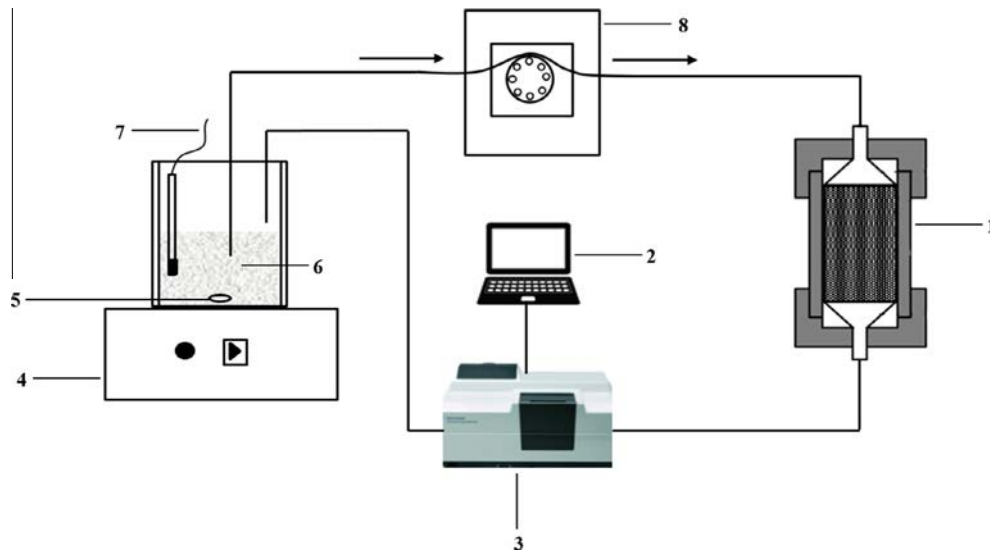


Fig. 1. Schematic of the experimental setup used to study the activity of bare and metal hydroxide precipitated sphalerite at alkaline pH for ethyl xanthate adsorption. 1. Fixed-bed adsorption reactor, 2. Computer controlling Cary WinUV software, 3. Cary 300 UV-visible spectrophotometer, 4. Magnetic stirring plate, 5. Magnetic stirrer, 6. Activator/collector solution, 7. pH-meter electrode, 8. Peristaltic pump.

conditions. Adsorption of ethyl xanthate on bare sphalerite was marginal as indicated by the limited collector uptake, *ca.* 3.8%, from the solution after adsorption equilibrium was attained. Adsorption of ethyl xanthate on un-activated sphalerite could be attributed to the presence of lattice copper and iron impurities as suggested from the analyses reported above in Section 2.1. Migration of copper impurities to the sphalerite surface, prompted by the initial acid washing pre-treatment, is indeed known to favor growth of copper-containing deficient sulfide surface species which constitute by themselves self-activation sites [27]. Also, the presence of surface ferrous iron could activate the sphalerite surface through formation of collector-ferric hydroxyl complexes responsible for the minor adsorption of ethyl xanthate on bare sphalerite [9]. Remarkably, the copper-hydroxide-doped sphalerite exhibited much more pronounced adsorption of ethyl xanthate. Collector uptake from the solution was very fast over the first 10 min of contact leading to the consumption of >95% ethyl xanthate followed by its complete disappearance after 30 min. In comparison with the copper hydroxides, ethyl xanthate adsorption on the iron hydroxide modified surface is considerably lower; after 50 min of

contact, collector concentration in the solution decreased by only *ca.* 13%. Unlikelihood of lattice replacement of zinc atoms by iron and copper at alkaline pH was verified by metal content analyses of the residual solutions after precipitation. Zinc went undetected in these solutions leading to the conclusion that the adsorption of iron and copper hydroxides on the sphalerite surface is in all appearance the main mechanism for collector adsorption.

3.2. Computational simulations

3.2.1. Iron & copper equilibrium speciation

Quantum mechanical simulations based on density functional theory prove to be a powerful tool to study electronic interactions between collectors and precipitated metal hydroxides along with the solution species in thermodynamic equilibrium with the metal hydroxides. At alkaline pH and in the absence of other complexing ligands, ferric iron and copper cations deprotonate the solvent leading to the formation of different iron and copper hydroxide complexes. The main complexation reactions and associated stability constants are shown in Table 1. The formation of different iron

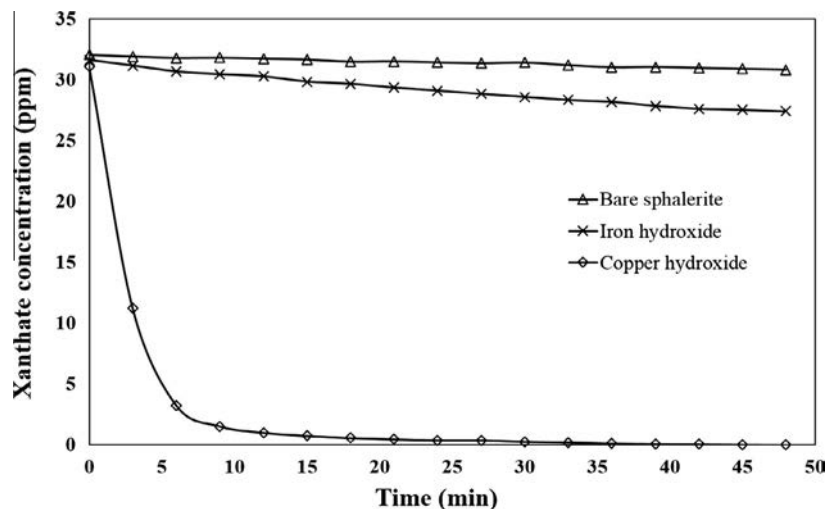


Fig. 2. Kinetics of ethyl xanthate anion adsorption on bare, and on iron and copper hydroxide doped sphalerite.

and copper hydroxide species at different pH values was calculated using the ChemEQL (version 3.0) Program [28]. This program takes into account all the chemical equilibria corresponding to the reaction schemes presented in Table 1 along with mass and charge neutrality balances to calculate the distributional speciation as a function of pH of the different iron and copper hydroxide species. Equilibrium calculations based on these stability constants revealed that precipitated $\text{Fe}(\text{OH})_3(\text{s})$ and $\text{Cu}(\text{OH})_2(\text{s})$ are the predominant phases formed at alkaline pH. However, depending on pH, these precipitates might involve equilibria with different metal hydroxide complexes, much plausibly within their electrical double layer. Figs. 3 and 4 display iron and copper speciation in terms of iron hydroxide and copper hydroxide complexes to form in the solution over the alkaline pH range. The main complex species in equilibrium with copper hydroxide precipitates is the soluble solvated $\text{Cu}(\text{OH})_2$ whereas the iron hydroxide precipitates are in equilibrium with both the solvated $\text{Fe}(\text{OH})_3$ and $\text{Fe}(\text{OH})_4^-$. At pH 10 coinciding with that for which the tests were performed, $\text{Fe}(\text{OH})_4^-$ anions are dominant species in equilibrium with the solid phase iron hydroxide. Due to the solubility of the precipitated copper and iron hydroxides, it could be assumed that ethyl xanthate is interacting with dissolved metal hydroxide complexes such as $\text{Cu}(\text{OH})_2$, $\text{Fe}(\text{OH})_3$ and $\text{Fe}(\text{OH})_4^-$ in the electrical double layer and then the resulting complexes are adsorbed on the metal hydroxide precipitates. The same mechanism has been reported for the adsorption of octyl hydroxymate collector on barite, calcite and bastnäsite in which the metal cation released from the mineral surfaces forms a metal hydroxyl complex and then interacts with the octyl hydroxymate collector in the electrical double layer before it is finally adsorbed on the mineral surface [29].

In order to help better understanding the mechanism of ethyl xanthate interaction with the species in equilibrium with the precipitated metal hydroxides, the following simulation considerations were further developed below. First, the structure of ethyl xanthate was optimized and the effect of water solvent molecules on its structure studied. The optimized solvated structure of aqueous $\text{Fe}(\text{OH})_3$ and $\text{Cu}(\text{OH})_2$ were then compared in terms of their interaction with ethyl xanthate. Finally, DFT simulation results on the interaction of ethyl xanthate with negatively-charged metal hydroxide complexes, e.g., $\text{Fe}(\text{OH})_4^-$ and $\text{Cu}(\text{OH})_3^-$ were discussed.

3.2.2. Optimized structure of solvated ethyl xanthate collector

The molecular structure of collector plays an important role in its interaction with the surface of mineral ores. Thus, the structures of ethyl xanthate were optimized through DFT simulations for different headspace environments. In absence of a solvation medium, the collector optimized structure is shown in Fig. 5a where the double and single sulfur-carbon bond lengths are 1.695 and 1.704 Å, respectively. These nearly similar bond lengths indicate that the electrons can transfer freely between the two S—C bonds. Electron from the negatively charged ethyl xanthate anion can be shared with the metal hydroxide complexes through a covalent bond where valence electron transfer takes place from the collector

Highest Occupied Molecular Orbital (HOMO). The ethyl xanthate HOMO, illustrated in Fig. 5b, shows that the transferable charge is located around the two sulfur atoms whereby their $3p_x$ and $3p_z$ atomic orbitals have the most significant contribution to the collector HOMO at the expense of the minor role of carbon and oxygen orbitals. Thus, the highest contribution to the collector covalent bonding with the metal hydroxide complexes very likely would stem from its two sulfur atoms.

In a flotation process, ethyl xanthate is surrounded by water molecules which could influence its properties. Therefore, the effect of solvation on the electrical and geometrical properties of the collector was investigated through DFT by the relaxation of water molecules around ethyl xanthate and the optimization of the solvated anion. The water molecules are interacting with the polar head of the ethyl xanthate collector through hydrogen bonding with the sulfur atoms. The hydrogen bond length between water molecules and sulfur atoms varies between 2.25 and 2.44 Å with an average length of 2.30 Å. Such interactions with solvent molecules lead to changes in the collector electrical and geometrical properties. The electrons being shared through hydrogen bond contribute to reduce the negative charges around the sulfur atoms. The Mulliken atomic charge distribution of solvated ethyl xanthate showed slightly lower negative charges around sulfur atoms (average charge -0.57) as compared with the solvent-free case (average charge -0.63). Solvation also leads to a slightly increased average S=C bond length, from 1.70 Å in vacuum to 1.72 Å under collector solvation, forecasting a slightly lowered electron donating ability in aqueous solution of ethyl xanthate.

3.2.3. Optimized structure of solvated $\text{Fe}(\text{OH})_3$ & $\text{Cu}(\text{OH})_2$

The DFT optimized $\text{Fe}(\text{OH})_3$ and $\text{Cu}(\text{OH})_2$ solvated by six water molecules are shown in Fig. 6a and b. From Fig. 6a, the $\text{Fe}(\text{OH})_3$ is interacting with six surrounding H_2O molecules through the formation of two covalent and several hydrogen bonds. The optimized solvated $\text{Fe}(\text{OH})_3$ has a molecular structure close to trigonal bipyramidal in which the two covalently bonded water molecules to iron form axial ligands while the three hydroxyl groups make the equatorial ligands located in a plane close to perpendicular to the axial axis with $\text{O}_{\text{ax}}-\text{Fe}-\text{O}_{\text{eq}}$ angle varying between 87.7° and 96.8° . The DFT analysis of the orbital's eigenvectors show that the two newly formed covalent bonds between Fe and oxygen atoms were the result of the overlap between Fe $3d$ and oxygen sp^3 hybridized orbitals. The formation of new covalent bonds was also confirmed through monitoring of the electron density difference between the obtained DFT computed electron density and the linear combination of atomic densities. As seen Fig. 6a, plot of the electron density difference field with 0.05 e iso-surface value shows the clear gain in electron density in the binding regions between oxygen and Fe atoms thereby confirming formation of new covalent bonds. However, the Mulliken charge distribution analysis of the individual atoms of the solvated $\text{Fe}(\text{OH})_3$ revealed that the two oxygen atoms in the axial coordinates involved in the sigma bonding with the two water molecules have less charge density (average of -0.52 e) than the equatorial oxygen atoms (average of -0.65 e). Furthermore, the average length of $\text{Fe}-\text{O}_{\text{ax}}$ bond was 2.0 Å which is considerably larger than that of $\text{Fe}-\text{O}_{\text{eq}}$ (1.86 Å). From these results, one can conclude that the two covalent bonds formed by the interaction of Fe and the surrounding water molecules are weaker than the bonds formed between the hydroxyl groups and Fe atoms.

The formation of two covalent bonds with the surrounding water molecules was also observed for the solvated $\text{Cu}(\text{OH})_2$ molecules (Fig. 6b). The solvated $\text{Cu}(\text{OH})_2$ also contributes two sigma bonding with the H_2O oxygen atoms leading to a disphenoidal shape for the solvated copper hydroxide. Unlike for the solvated $\text{Fe}(\text{OH})_3$, the hydroxyl groups in the solvated $\text{Cu}(\text{OH})_2$ are

Table 1
Stability constants for Fe^{3+} and Cu^{2+} speciations.

Reactions	Stability constants ($\text{Log}_{10}(K)$)
$\text{Fe}^{3+} + 3\text{H}_2\text{O} \leftrightarrow 3\text{H}^+ + \text{Fe}(\text{OH})_3(\text{s})$	-3.2
$\text{Fe}^{3+} + \text{H}_2\text{O} \leftrightarrow \text{H}^+ + \text{Fe}(\text{OH})^{2+}$	-2.19
$\text{Fe}^{3+} + 2\text{H}_2\text{O} \leftrightarrow 2\text{H}^+ + \text{Fe}(\text{OH})_2^+$	-5.67
$\text{Fe}^{3+} + 3\text{H}_2\text{O} \leftrightarrow 3\text{H}^+ + \text{Fe}(\text{OH})_3$	-12.56
$\text{Fe}^{3+} + 4\text{H}_2\text{O} \leftrightarrow 4\text{H}^+ + \text{Fe}(\text{OH})_4^-$	-21.6
$\text{Cu}^{2+} + 2\text{H}_2\text{O} \leftrightarrow 2\text{H}^+ + \text{Cu}(\text{OH})_2(\text{s})$	-8.68
$\text{Cu}^{2+} + \text{H}_2\text{O} \leftrightarrow \text{H}^+ + \text{Cu}(\text{OH})^+$	-7.7
$\text{Cu}^{2+} + 2\text{H}_2\text{O} \leftrightarrow 2\text{H}^+ + \text{Cu}(\text{OH})_2$	-13.68
$\text{Cu}^{2+} + 3\text{H}_2\text{O} \leftrightarrow 3\text{H}^+ + \text{Cu}(\text{OH})_3^-$	-26.9

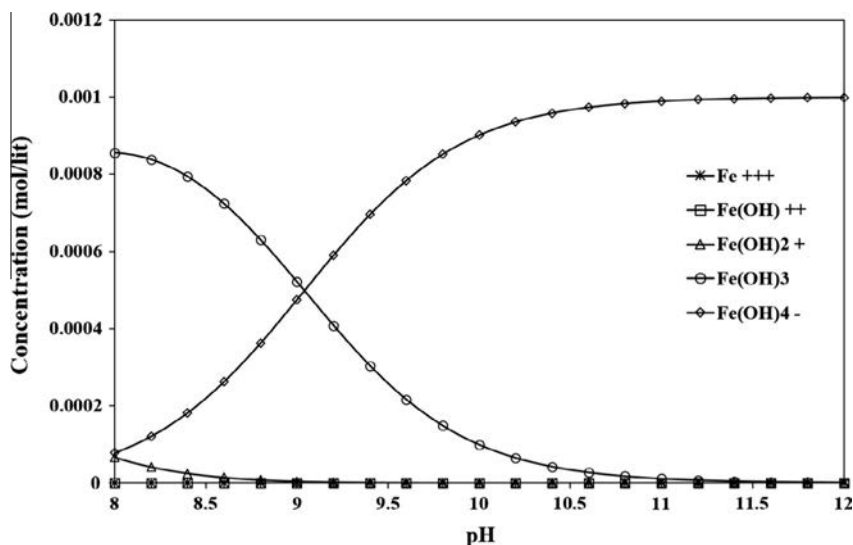


Fig. 3. Concentration of different iron hydroxide complexes in solutions as a function of pH. Total Fe^{3+} concentration in solution = 1 mM.

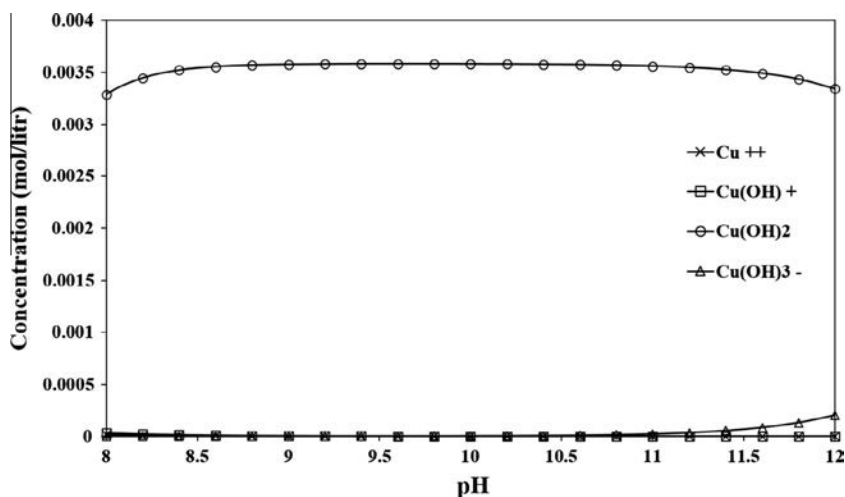


Fig. 4. Concentration of different copper hydroxide complexes in solutions as a function of pH. Total Cu^{2+} concentration in solution = 3.6 mM.

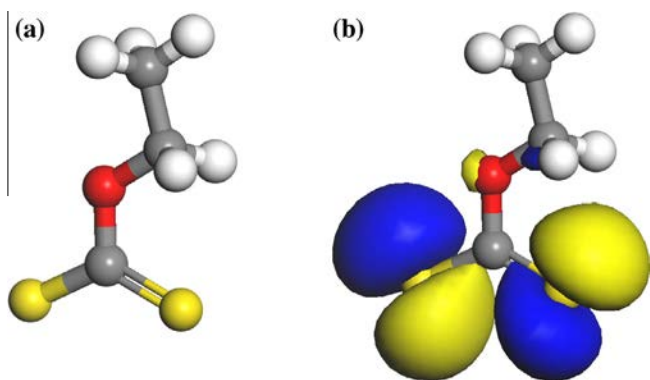


Fig. 5. DFT-optimized structure of non-solvated ethyl xanthate anion (a), Highest Occupied Molecular Orbital (HOMO) of non-solvated ethyl xanthate anion (b), (S \equiv yellow, O \equiv red, C \equiv gray, H \equiv white). (For interpretation of the references to colour in this figure legend, the reader is referred to the web version of this article.)

positioned in the axial axes to form axial ligands. The $\text{O}_{\text{ax}}-\text{Cu}-\text{O}_{\text{ax}}$ angle is about 175° which is smaller than the ideal axial angle in a disphenoidal structure (180°). The two water ligands are then

forming equatorial ligands with $\text{O}_{\text{eq}}-\text{Cu}-\text{O}_{\text{eq}}$ angle of 143.0° . Similar to the solvated $\text{Fe}(\text{OH})_3$, the copper atoms contribute stronger covalent bonds with the OH oxygen atoms than with water molecules. The average bond length of $\text{Cu}-\text{O}_{\text{water}}$ is 2.14 \AA which is considerably larger than that of $\text{Cu}-\text{O}_{\text{hydroxyl}}$ (1.92 \AA). In addition, the Mulliken charge difference between the $\text{Cu}-\text{O}_{\text{hydroxyl}}$ ($-1.17 e$) was higher than that of $\text{Cu}-\text{O}_{\text{water}}$ ($-0.99 e$) indicating the former stronger bonding.

3.2.4. Interaction of ethyl xanthate with solvated $\text{Fe}(\text{OH})_3$ & $\text{Cu}(\text{OH})_2$

In order to obtain the optimum configuration for the interaction of ethyl xanthate collector with solvated $\text{Fe}(\text{OH})_3$ and $\text{Cu}(\text{OH})_2$ molecules, several DFT optimizations were performed by placing the ethyl xanthate molecule at different locations around the solvated metal hydroxides with six water molecules and the optimum configurations obtained for the collector interaction with the solvated $\text{Fe}(\text{OH})_3$ and $\text{Cu}(\text{OH})_2$ molecules are shown in Fig. 7a and b, respectively. The interaction of ethyl xanthate with solvated $\text{Fe}(\text{OH})_3$ leads to the formation of a covalent bond between a sulfur atom of the collector polar head and the Fe atom with an interaction energy of -161.3 kJ/mol (Fig. 7a). The sulfur atoms of the ethyl xanthate anion could also make hydrogen

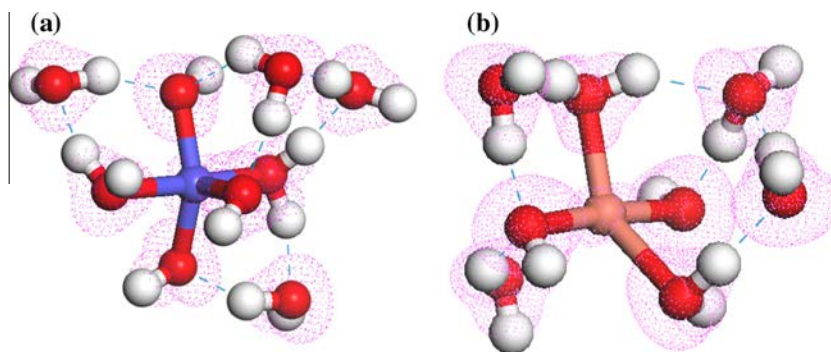


Fig. 6. DFT-optimized structure of solvated $\text{Fe}(\text{OH})_3$ (a) and $\text{Cu}(\text{OH})_2$ (b) in the presence of six water molecules (Fe \equiv blue, Cu \equiv purple). The electron density difference field with 0.05 e iso-surface value also shown. (For interpretation of the references to colour in this figure legend, the reader is referred to the web version of this article.)

bounds with the hydrogen atoms of the solvated $\text{Fe}(\text{OH})_3$ which helps stabilizing the ethyl xanthate-solvated metal hydroxide complex as well. The new complex formed due to this interaction has a close to octahedral structure in which ethyl xanthate is bounded axially with the iron atom of the solvated $\text{Fe}(\text{OH})_3$ with an Fe–S bond length of 2.37 Å. The interaction of ethyl xanthate with the solvated $\text{Fe}(\text{OH})_3$ resulted in considerable changes in the strength of the Fe– $\text{O}_{\text{hydroxyl}}$ and Fe– O_{water} bonds. Due to the negative charge carried by ethyl xanthate anion, the Mulliken electron density around the Fe atom increased from +0.72 to +0.51 e. This increase in electron density around Fe atoms resulted in the rise of the average bond length of Fe– $\text{O}_{\text{hydroxyl}}$ from 1.83 Å (solvated $\text{Fe}(\text{OH})_3$) to 1.93 Å (after interaction with ethyl xanthate) as well as the increase in the average bond length of Fe– O_{water} from 2.0 Å to 2.10 Å indicating that the bond strength reduced considerably. However, the solvated $\text{Fe}(\text{OH})_3$ kept its covalent bonds with the hydroxyl groups and the two water molecules after it interacted with ethyl xanthate.

The optimized structure of solvated $\text{Cu}(\text{OH})_2$ after interaction with ethyl xanthate collector is shown in Fig. 7b. As can be seen, ethyl xanthate collector is interacting with the solvated $\text{Cu}(\text{OH})_2$ through formation of two covalent bonds between the collector sulfur atoms and copper with an average bond length of 2.41 Å. Contrarily to the solvated $\text{Fe}(\text{OH})_3$ complex, the interaction of solvated $\text{Cu}(\text{OH})_2$ with ethyl xanthate led to the removal of weakly covalent bonds between $\text{Cu}(\text{OH})_2$ and the two water molecules.

The interaction of solvated $\text{Cu}(\text{OH})_2$ with ethyl xanthate decreased the total system energy by -217.1 kJ/mol. In the absence of ethyl xanthate collector, the removal of the two covalent bonds between water molecules and $\text{Cu}(\text{OH})_2$ increases the total energy of the system by about +120 kJ/mol. Consequently, it could be concluded that the formation of covalent bond between the two sulfur atoms of ethyl xanthate and copper could lead to the reduction of the total energy by *ca.* -335 kJ/mol. The DFT simulations reveal that the interaction of ethyl xanthate with solvated $\text{Cu}(\text{OH})_2$ could be more energetically favorable than that of ethyl xanthate with solvated $\text{Fe}(\text{OH})_3$. In addition, the simulations indicate that the interaction energy of ethyl xanthate with non-solvated $\text{Cu}(\text{OH})_2$ is about -148.3 kJ/mol which is considerably lower than that in the presence of solvent. The Mulliken charge distribution analysis indicates that the solvation of copper hydroxide and formation of hydrogen bonds between the hydroxyl groups and surrounding water molecules reduces considerably the electron density around the copper atoms (+0.39 e for non-solvated copper hydroxides vs. +0.56 e for the solvated one). This results in increased strength of the covalent bonds between copper and sulfur atoms in the solvating medium.

In order to calculate the energy barriers for the interaction of ethyl xanthate anion with solvated $\text{Fe}(\text{OH})_3$ and $\text{Cu}(\text{OH})_2$, the transition state search was performed using the complete LST/QST method. In this method, first a single LST maximization is performed to bracket the maximum energy between the reactants

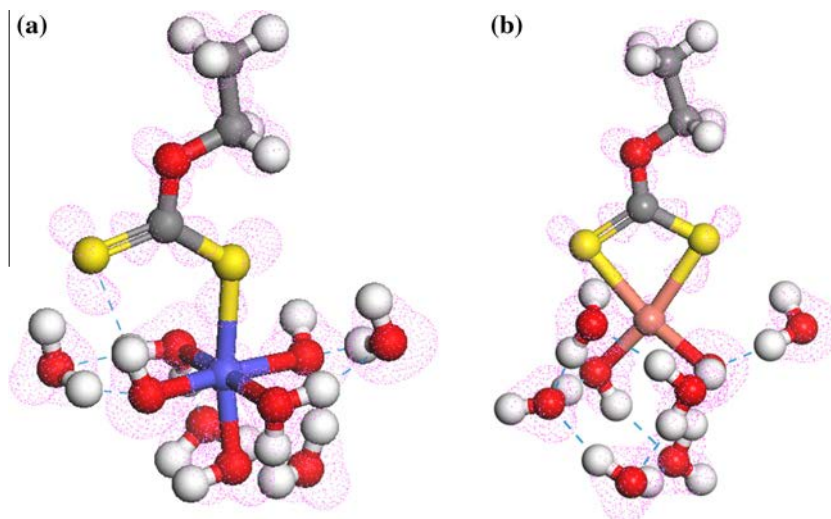


Fig. 7. DFT-optimized structures resulting from interaction of an ethyl xanthate anion with solvated $\text{Fe}(\text{OH})_3$ (a) and $\text{Cu}(\text{OH})_2$ (b) in the presence of six water molecules. The electron density difference field with 0.05 e iso-surface value also shown.

and products followed by energy minimization in conjugate directions to reaction pathway leading to a structure lower in energy and closer to the true transition state. This structure is then used as an approximation to perform a QST maximization followed by another conjugate gradient minimization. The results of our transition state search showed that the barrier energy for the interaction of ethyl xanthate anion with the solvated $\text{Fe}(\text{OH})_3$ was *ca.* +18.3 kJ/mol. The transition state resulting from the interaction of ethyl xanthate anion and solvated $\text{Cu}(\text{OH})_2$ had almost the same energy as the reactants and the energy barrier was less than 10 kJ/mol. Such low-energy barriers suggest that the interaction between ethyl xanthate and both solvated metal hydroxides is not kinetically limited.

The possibility of interaction of a second ethyl xanthate anion with a solvated copper or iron hydroxide was investigated by locating and relaxing a second ethyl xanthate at different initial positions around the optimized configurations previously obtained. The most stable configuration resulted from the interaction of two ethyl xanthate anions and the solvated $\text{Fe}(\text{OH})_3$ and $\text{Cu}(\text{OH})_2$ in the presence of four water molecules are presented in Fig. 8a and b, respectively. As can be seen in these figures, the DFT simulations reveal that the interaction of solvated $\text{Fe}(\text{OH})_3$ and $\text{Cu}(\text{OH})_2$ with two ethyl xanthate molecules is energetically possible. Due to this interaction, the two ethyl xanthate anions are bonded to the solvated $\text{Fe}(\text{OH})_3$ or $\text{Cu}(\text{OH})_2$ through the formation of a covalent bond between one of their sulfur atoms and the transition metal. These interactions also result into the removal of the covalent bonds between the metal hydroxide and the surrounding water molecules. However, the decrease in the total energy of the system due to the interaction of the second ethyl xanthate molecule with the solvated $\text{Fe}(\text{OH})_3$ and $\text{Cu}(\text{OH})_2$ was less than -20 kJ/mol.

3.2.5. Effect of OH^- groups on interaction of ethyl xanthate with solvated $\text{Fe}(\text{OH})_3$ & $\text{Cu}(\text{OH})_2$

The presence at alkaline pH of hydroxide anions around the solvated $\text{Fe}(\text{OH})_3$ and $\text{Cu}(\text{OH})_2$ hydroxides could influence their interaction with ethyl xanthate. In order to study this effect, first the influence of OH^- groups on the interaction of ethyl xanthate molecule with $\text{Fe}(\text{OH})_3$ or $\text{Cu}(\text{OH})_2$ in the absence of solvent around the metal hydroxides was studied. The OH^- and ethyl xanthate groups were located at different positions around the iron and copper

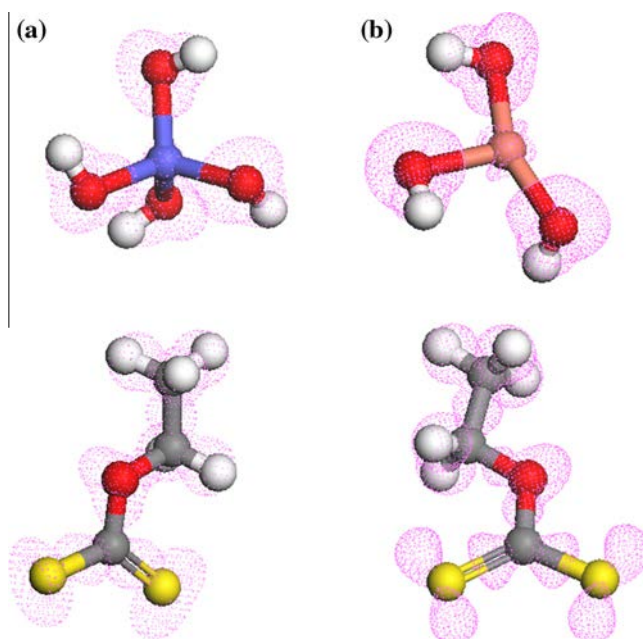


Fig. 9. DFT-optimized structure obtained from the relaxation of ethyl xanthate anion and a hydroxyl group around solvated $\text{Fe}(\text{OH})_3$ (a) and $\text{Cu}(\text{OH})_2$ (b) in absence of water molecules. The electron density difference field with 0.05 e iso-surface value also shown.

hydroxide entities and the most stable configurations were obtained through the DFT optimization. As can be observed in Fig. 9a and b, the OH^- group is interacting with $\text{Fe}(\text{OH})_3$ and $\text{Cu}(\text{OH})_2$ through formation of a covalent bond between its oxygen atom and iron and copper metals leading to the formation of, respectively, $\text{Fe}(\text{OH})_4^-$ and $\text{Cu}(\text{OH})_3^-$ while ethyl xanthate is excluded from having an interaction with the metal hydroxide. The interaction of $\text{Fe}(\text{OH})_3$ and $\text{Cu}(\text{OH})_2$ with OH^- groups resulted in more energetically stable configurations than with ethyl xanthate. The interaction of OH^- groups with $\text{Fe}(\text{OH})_3$ or $\text{Cu}(\text{OH})_2$ and the formation of $\text{Fe}(\text{OH})_4^-$ and $\text{Cu}(\text{OH})_3^-$ led to -400.0 kJ/mol and -374.9 kJ/mol reduction in the total energy of the system, respectively. Likewise, the interaction of iron and copper hydroxides with ethyl xanthate in the absence of solvent only reduced

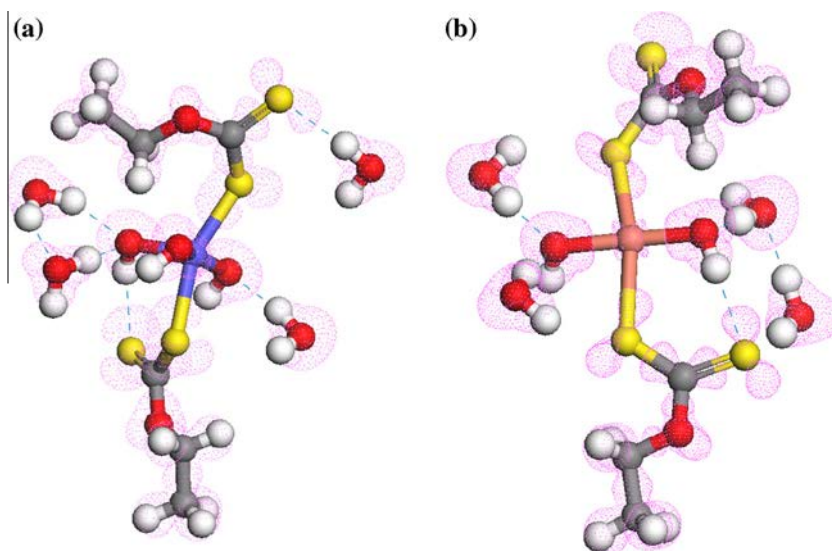


Fig. 8. DFT-optimized structure resulting from the interaction of two ethyl xanthate anions with solvated $\text{Fe}(\text{OH})_3$ (a) and $\text{Cu}(\text{OH})_2$ (b) in the presence of 4 water molecules. The electron density difference field with 0.05 e iso-surface value also shown.

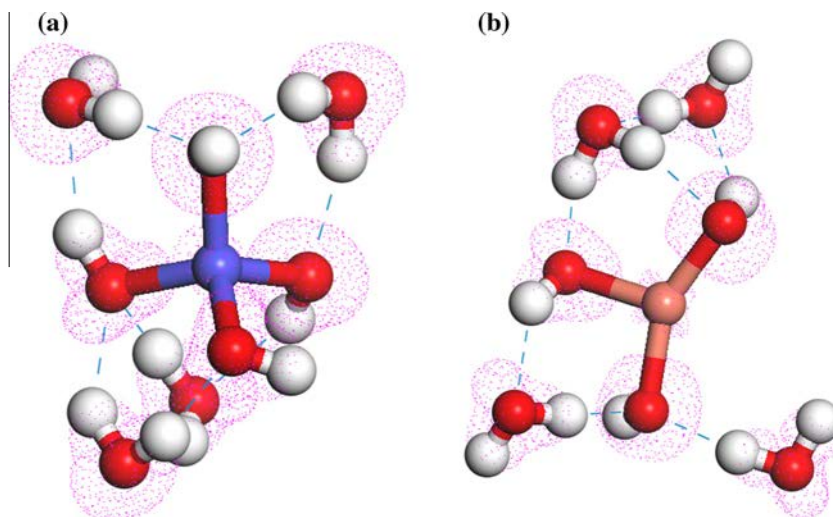


Fig. 10. DFT-optimized structure obtained from the relaxation of a hydroxyl group around solvated $\text{Fe}(\text{OH})_3$ (a) and $\text{Cu}(\text{OH})_2$ (b) in the presence of 4 water molecules. The electron density difference field with 0.05 e iso-surface value also shown.

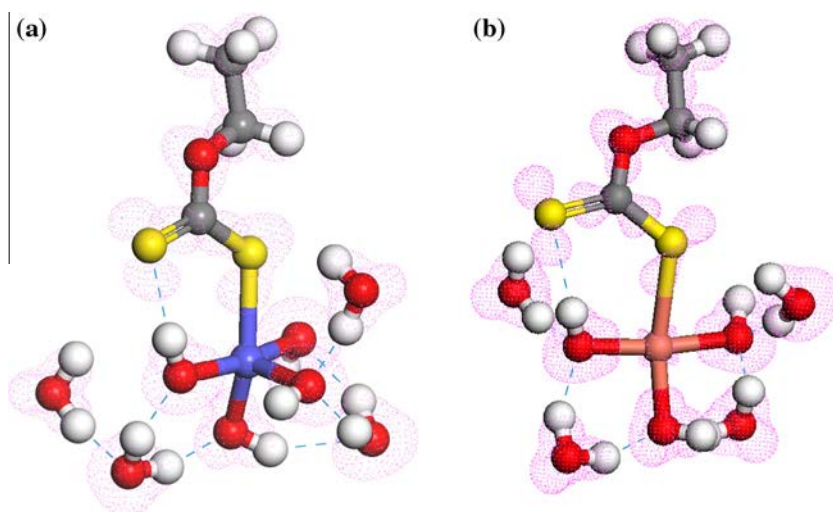


Fig. 11. DFT-optimized structure obtained from the relaxation of an ethyl xanthate anion and a hydroxyl group around solvated $\text{Fe}(\text{OH})_3$ (a) and $\text{Cu}(\text{OH})_2$ (b) in the presence of 4 water molecules. The electron density difference field with 0.05 e iso-surface value also shown.

to -148.3 kJ/mol and -203.1 kJ/mol, respectively, of the total system energy. Consequently, it may be concluded that the interactions of $\text{Fe}(\text{OH})_3$ or $\text{Cu}(\text{OH})_2$ with OH^- groups are more thermodynamically favorable than those with ethyl xanthate.

The interaction of OH^- and ethyl xanthate groups with solvated copper and iron hydroxides was also investigated through DFT simulations. In the absence of ethyl xanthate, the OH^- groups are interacting with the solvated $\text{Fe}(\text{OH})_3$ and $\text{Cu}(\text{OH})_2$ resulting in the formation of new covalent bonds between the metal hydroxides and OH^- group. Fig. 10a and b shows the DFT optimized configuration of four H_2O -solvated $\text{Fe}(\text{OH})_3$ and $\text{Cu}(\text{OH})_2$ after interaction with an OH^- group. As seen in these figures, the interaction of OH^- with the solvated metal hydroxides resulted in the removal of covalent bonds between water molecules and $\text{Fe}(\text{OH})_3$ and $\text{Cu}(\text{OH})_2$. The formed $\text{Fe}(\text{OH})_4^-$ and $\text{Cu}(\text{OH})_3^-$ complexes are then solvated through the formation of hydrogen bonding between the surrounding water molecules and the hydroxyl groups of the metal hydroxides. The interaction of OH^- group with the solvated $\text{Fe}(\text{OH})_3$ and $\text{Cu}(\text{OH})_2$ led to -462.6 kJ/mol and -393.9 kJ/mol reduction in the total system energy showing the high thermodynamic affinity of the metal hydroxides to interact with OH^- groups.

The DFT simulations also showed that the ethyl xanthate anion could interact with the solvated $\text{Fe}(\text{OH})_4^-$ and $\text{Cu}(\text{OH})_3^-$ complexes. Fig. 11a and b reveals that the interaction of ethyl xanthate anion with the solvated $\text{Fe}(\text{OH})_4^-$ and $\text{Cu}(\text{OH})_3^-$ takes place through the formation of a covalent bond between the collector sulfur atoms and the transition metals. However, the resulting decrease in system's total energy between ethyl xanthate and $\text{Fe}(\text{OH})_4^-$ and $\text{Cu}(\text{OH})_3^-$ complexes was less than -20 kJ/mol showing that the extent of this interaction is thermodynamically limited.

4. Conclusion

Quantum mechanical simulations based on density functional theory were performed in this study in an attempt to interpret experimental observations regarding the interaction of ethyl xanthate with precipitated iron and copper hydroxides at alkaline pH. The DFT simulations showed that the interaction of neutral-charge $\text{Fe}(\text{OH})_3$ and $\text{Cu}(\text{OH})_2$ complexes with ethyl xanthate is energetically and thermodynamically favorable while negatively-charged complexes such as $\text{Fe}(\text{OH})_4^-$ and $\text{Cu}(\text{OH})_3^-$ are barely

interacting with the collector. Phase equilibria calculations at the tested alkaline pH showed that $\text{Fe}(\text{OH})_4^-$ complexes are the dominant species in equilibrium with $\text{Fe}(\text{OH})_3$ precipitate phase. Their less favorable interaction with ethyl xanthate anion could be at the origin of the lower collector affinity towards iron hydroxides. Conversely, the aqueous $\text{Cu}(\text{OH})_2$ found in the electrical double layer around has a considerable affinity for the interaction with ethyl xanthate.

References

- [1] S. Ata, *Int. J. Miner. Process.* 102 (2012) 1–12.
- [2] B. Wang, Y. Peng, *Miner. Eng.* 66–68 (2014) 13–24.
- [3] M.C. Biesinger, B.R. Hart, R. Polack, B.A. Kobe, R.S.C. Smart, *Miner. Eng.* 20 (2007) 152–162.
- [4] S.C. Chelgani, B. Hart, *Miner. Eng.* 57 (2014) 1–11.
- [5] W. Tolley, D. Kotlyar, R. VanWagoner, *Miner. Eng.* 9 (1996) 603–637.
- [6] J.-S. Deng, Y.-B. Mao, S.-M. Wen, J. Liu, Y.-J. Xian, Q.-C. Feng, *Int. J. Miner. Metall. Mater.* 22 (2015) 111–115.
- [7] C. Owusu, J. Addai-Mensah, D. Fornasiero, M. Zanin, *Adv. Powder Technol.* 24 (2013) 801–809.
- [8] C. Owusu, D. Fornasiero, J. Addai-Mensah, M. Zanin, *Int. J. Miner. Process.* 134 (2015) 50–57.
- [9] A.P. Chandra, A.R. Gerson, *Adv. Colloid Interface Sci.* 145 (2009) 97–110.
- [10] E.T. Pecina, A. Uribe, F. Nava, J.A. Finch, *Miner. Eng.* 19 (2006) 172–179.
- [11] Y.J. Peng, B. Wang, A. Gerson, *Int. J. Miner. Process.* 102 (2012) 141–149.
- [12] W.J. Trahar, G.D. Senior, G.W. Heyes, M.D. Creed, *Int. J. Miner. Process.* 49 (1997) 121–148.
- [13] N.P. Finkelstein, *Int. J. Miner. Process.* 52 (1997) 81–120.
- [14] Z. Ekmekci, H. Demirel, *Int. J. Miner. Process.* 52 (1997) 31–48.
- [15] D. Fornasiero, J. Ralston, *J. Colloid Interface Sci.* 151 (1992) 225–235.
- [16] S. He, W. Skinner, D. Fornasiero, *Int. J. Miner. Process.* 80 (2006) 169–176.
- [17] S. Grano, *Miner. Eng.* 22 (2009) 386–394.
- [18] D. Fornasiero, V. Eijt, J. Ralston, *Colloids Surf.* 62 (1992) 63–73.
- [19] J.H. Chen, Y.Q. Li, C.H. Zhao, *Comput. Mater. Sci.* 88 (2014) 1–6.
- [20] A. Azizi, C.F. Petre, C. Olsen, F. Larachi, *Hydrometallurgy* 107 (2011) 101–111.
- [21] C.I. Basilio, I.J. Kartio, R.H. Yoon, *Miner. Eng.* 9 (1996) 869–879.
- [22] J. Liu, S.M. Wen, J.S. Deng, X.M. Chen, Q.C. Feng, *Appl. Surf. Sci.* 311 (2014) 258–263.
- [23] C.C. Sui, S.H.R. Brienne, Z.H. Xu, J.A. Finch, *Int. J. Miner. Process.* 49 (1997) 207–221.
- [24] J. Scaranto, S. Giorgianni, *Comput. Mater. Sci.* 81 (2014) 556–560.
- [25] W.J. Qi, J.Y. Ran, R.R. Wang, X.S. Du, J. Shi, M.C. Ran, *Comput. Mater. Sci.* 111 (2016) 430–442.
- [26] M.D. Ganji, N. Sharifi, M.G. Ahangari, *Comput. Mater. Sci.* 92 (2014) 127–134.
- [27] A.N. Buckley, R. Woods, H.J. Wouterlood, *Int. J. Miner. Process.* 26 (1989) 29–49.
- [28] B. Muller, *ChemEQL*, V. 3.0, a Program to Calculate Chemical Speciation and Chemical Equilibria, EAWAG, Switzerland, 2004.
- [29] Pradip, D.W. Fuerstenau, *Colloids Surf.* 8 (1983) 103–119.